

SABSOON SCIENCE REPORT – NOVEMBER 2000

SABSOON group – H. Seim, J. Nelson, J. Bane, J. Blanton, F. Werner, C. Barans, R. Jahnke, M. Moran, R. Zepp, G. Paffenhöfer

Introduction

The South Atlantic Bight Synoptic Offshore Observational Network (SABSOON) was conceived as a long-term coastal observatory centrally located on the continental shelf of the southeastern United States. Motivation for this observatory came from several sources, including the growing and important needs for coastal ocean observations over long time scales, the importance of real-time over-water measurements to aid in severe weather prediction, and the availability of a network of existing fixed platforms on which to mount instrumentation and communications systems.

Implementation of SABSOON began in the fall of 1998 with funding from the National Oceanographic Partnership Program (NOPP). The network takes advantage of a U.S. Navy Tactical AirCrew Combat Training System (TACTS), a training facility that consists of a grid of eight unmanned, autonomous oil-rig-like platforms interconnected by a high bandwidth wireless communications system (Figure 1). SABSOON is deploying oceanographic and meteorological instrument on the platforms and utilizing the TACTS communications system to create a distributed real-time coastal ocean observing system. Data collection at SABSOON began in June 1999.

The intent of this report is to provide an overview of the measurements being collected and the scientific results to date. After outlining the status of the network at the time of writing, subsequent sections describe results from the various instrument systems that have been deployed, illustrating the potential of the network to provide new and fundamental information about the coastal ocean.

System Status

While the TACTS system has provided the critical infrastructure for the offshore network, all the components of SABSOON had to be designed, built and deployed. To gain confidence in the design of systems developed for SABSOON, Phase One of the project fully instrumented one platform, (tower R2, see Figure 1) and established the communications system and data archiving system. The implementation strategy of SABSOON and a detailed description of the instrument systems are given in Seim (2000). Collection of meteorological observations began in June 1999 and the tower was fully instrumented with meteorological and in-water sensors, an underwater video camera system (for fisheries research), and robust data acquisition system by November, 1999. Data loss due to communications problems since this time has been less than 1%.

Phase Two of the project is extending the network to multiple platforms, starting with towers M2 and R8. Power and communications were established at M2 in March, 2000. An upward looking acoustic doppler current profiler (ADCP), connected by cabling to the tower, was deployed roughly 200 m from the tower and has been reporting currents since mid-April, 2000. An in-water sensor system, described in Seim (2000), was deployed in early September 2000, and completes initial

instrumentation of M2. Variables observed include near surface and near bottom ocean temperature, salinity, pressure, *Chlorophyll A* fluorescence and photosynthetically available radiation, and bottom optical transmissometry, and ocean currents and acoustic backscatter strength (at 300 kHz) at 1 m intervals between the ocean surface and seafloor.

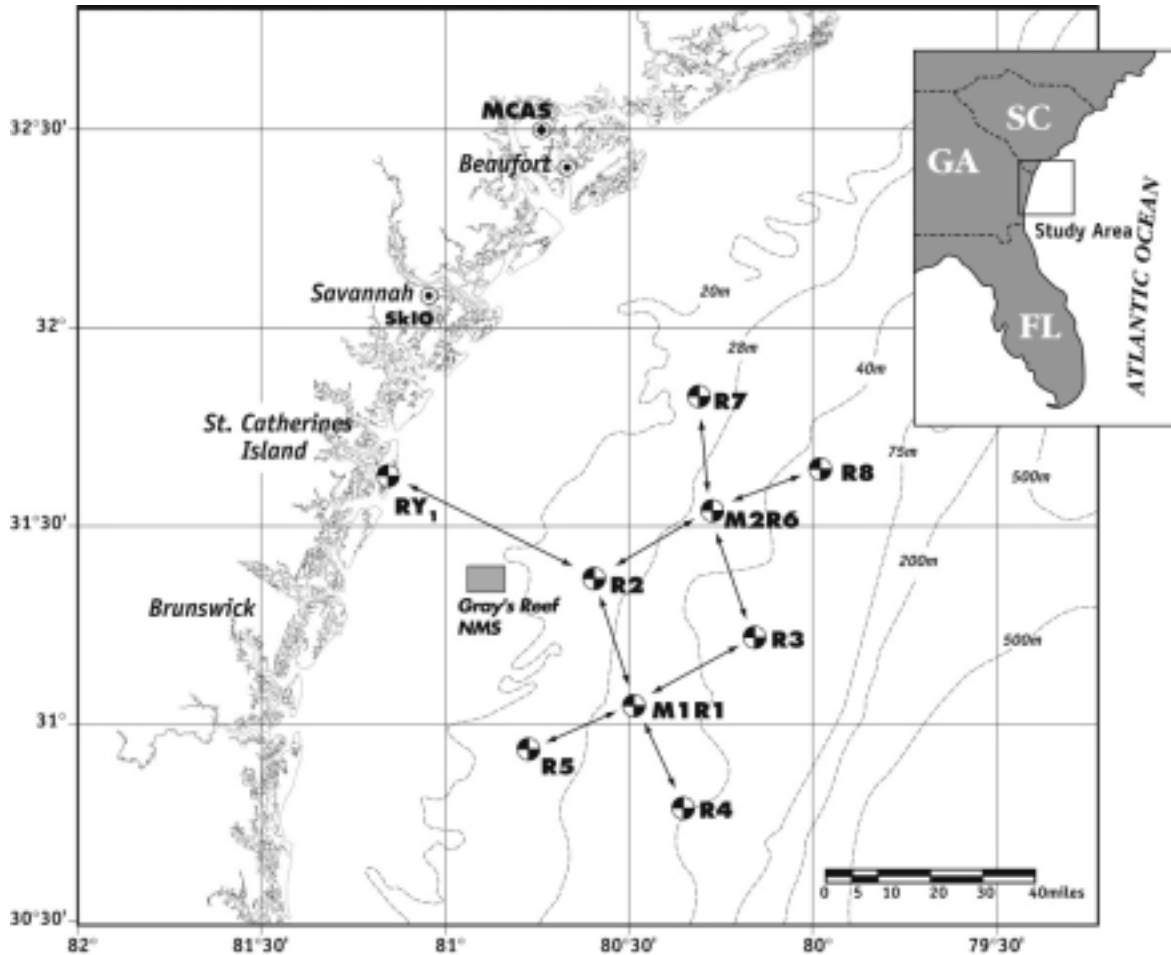


Figure 1. Map of the Georgia shelf showing the locations and names of the towers that make up the TACTS system.

The other component of phase 2 requires the design, construction and deployment of independent power and communications for tower R8. The larger “master” towers R2, M1 and M2, have sufficient excess power and communications bandwidth in the Navy system to accommodate the basic SABSOON requirements. This is not the case at tower R8 and the four other “remote” towers. Design of the SABSOON power and communications systems for the “remote” platforms was completed in August 2000, and construction and deployment of these systems at R8 will continue through the Fall.

Marine Meteorology

Two meteorological packages, modeled after the IMET system (Hosom et al., 1995) are deployed at R2. The primary package (including radiometry) is installed on the top of the tower structure, approximately 50 m above the water surface, and has been operational since June 1999. The secondary package is installed on a grating stairway on the northern side of the tower 10 m above the water, and has been operational since November 1999. The primary package was installed at the top of the structure to reduce the influence of flow distortion (Cooper et al, 1993) and the secondary package provides observations at a standard height to assess the impact of the primary measurements being far removed from the water surface. Comparisons between measurements from the two levels will be made for periods when the lower package was not in the lee of the tower.

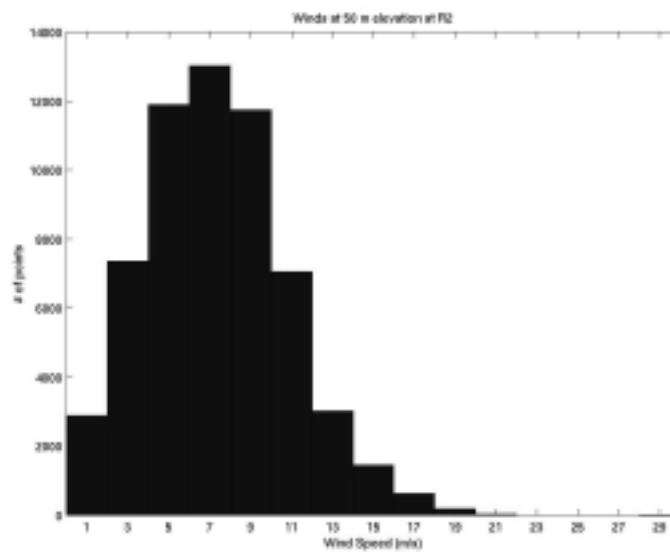


Figure 2. Histogram of winds speeds measured at 50 m from tower R2 between June 1, 1999 and June 30, 2000. All observations greater than 30 m/s are included in the greatest wind speed bin. Winds are typically 5-10 m/s.

Climatology observed over the last year is generally consistent with previous studies (e.g. Weber and Blanton, 1980). Wind speeds are typically 0-20 m/s, the majority being 5-10 m/s (Figure 2). The dominant wind direction is from the NE during mariner's fall and winter (October - March) and from the SW during the rest of the year (Figure 3). Air temperatures follow a seasonal cycle, being lowest in February, when temperature variance is also highest, associated with passage of wintertime frontal systems. Relative humidity averages 75%, the lowest values occurring between October and February.

Three hurricanes passed with 100 km of R2 in 1999 - Dennis, Floyd and Irene. Each produced pressures below 1000 mb and winds in excess of 20 m/s. Communications problems that were not solved until November 1999 prevented continuous data collection, but only small data gaps are present for hurricane Irene (Figure 4). Surface wave measurements were also collected and show a remarkably high correlation with wind speed. Most surprising is the abrupt drop in significant wave height coincident with the decrease in wind speed.

Maximum wind speeds observed since installation have been associated not with hurricanes but instead with the passage of squall lines and thunderstorms. On 9 occasions between July 1999 and June 2000 extreme wind events occurred that were associated with a rapid decrease in temperature, downpours, high-frequency barometric pressure fluctuations (> 1 cph) and 6-minute averaged wind speeds of 40-60 m/s (Figure 5). A series of wind maxima tend to occur over the duration of the events. The strong downdrafts (inferred from the drop in air temperatures), and wave-like pressure and wind speed are consistent with the atmospheric fronts experiencing non-linear steepening and evolving into soliton-like features. The consistency of the characteristics during all seasons suggests the mechanisms that lead to its evolution are quite robust.

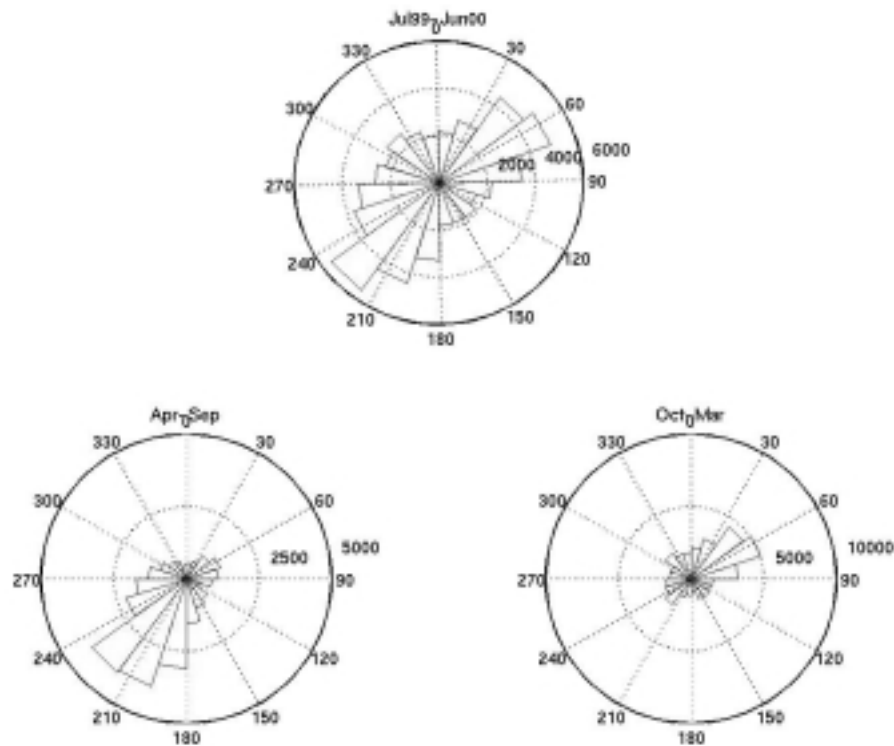


Figure 3. Wind direction (shown are direction the winds are blowing from) for June 1999 – June 2000 (top), June-September 1999 and April-June 2000 (left) and October 1999 – March 2000. The seasonal shift from southwesterly winds in the summer to northeasterly winds during mariner’s fall and winter is remarkably clear.

Heat flux into the ocean has been calculated from the meteorological observations (following e.g. Weller and Anderson, 1996) and integrated, assuming the mixed layer occupies the entire water column, to produce an estimate of the evolution of the ocean temperature. This 1-D model provides both a consistency check on the observations and a real-time estimate of departures from this simple balance (due, for example, to advection). Over the winter months the predicted temperature was a good estimate of observed ocean temperature (Figure 6), and departures from the prediction show a correlation with salinity variations. Cross-shelf transects and satellite imagery

revealed a cross-shelf gradient in temperature and salinity, both being lower at the coast. Salinities were low when observed temperatures were below the prediction and vice versa, suggesting cross-shelf advection of 5-10 km over time scales of 1-3 weeks. Forcing of these cross-isobath flows is not clear at this time; there is not an obvious correlation with the winds.

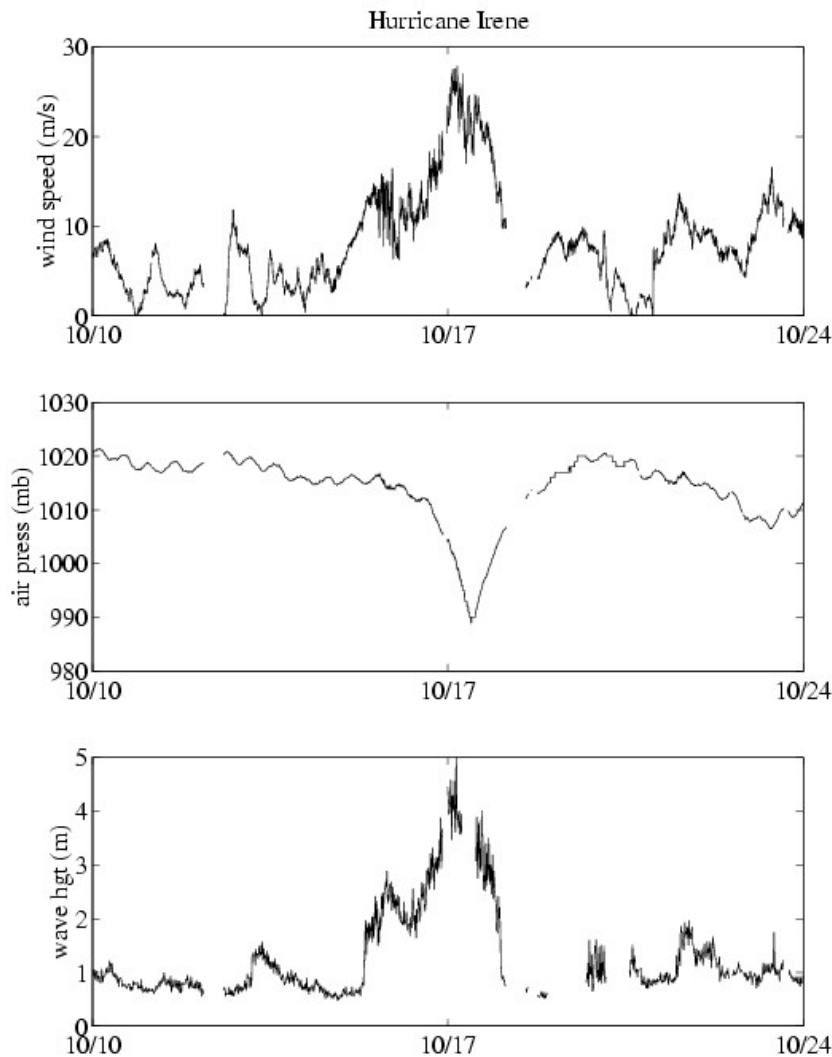


Figure 4. Six-minute average wind speed, air pressure and significant wave height at tower R2 during the passage of Hurricane Irene in October 1999. Peak sustained winds exceed 25 m/s, and peak wave heights reach 4.5 m. Note the remarkably rapid decrease in wave height as soon as the wind speeds decrease.

Since April 2000 the predicted temperature using observations from the primary meteorological package 50 m above the water is systematically lower than the observed temperatures. Replacing the air temperature and humidity readings with those from the secondary package 10 m above the water surface yields a better prediction (Figure 6, right). Stable atmospheric conditions during the spring can lead to considerable stratification in the marine boundary layer. Existing bulk formula can not account for this effect and the heat flux computed using the air measurements closer to the ocean surface is preferable.

Meteorological conditions were observed on the shelf-wide scale on several occasions using an instrumented aircraft. Information was collected throughout a 100 km x 200 km area encompassing the eight TACTS towers on four flights during the spring and summer of 2000. Near-surface wind, temperature and humidity fields were measured, as were oceanic temperatures to depths of 350 m (or the bottom, if shallower) using AXBTs and a sea surface temperature radiometer (Figures 7 and 8). Additionally, vertical profiles of the meteorological variables were made in the central tower area from 50 m to 1500 m altitude. These flights were made to assess the utility of this data collection method for periodically gaining wider spatial coverage in SABSOON, and to provide data for initialization and verification of circulation models. Initial study of the data shows that these surveys promise to be effective for both purposes.

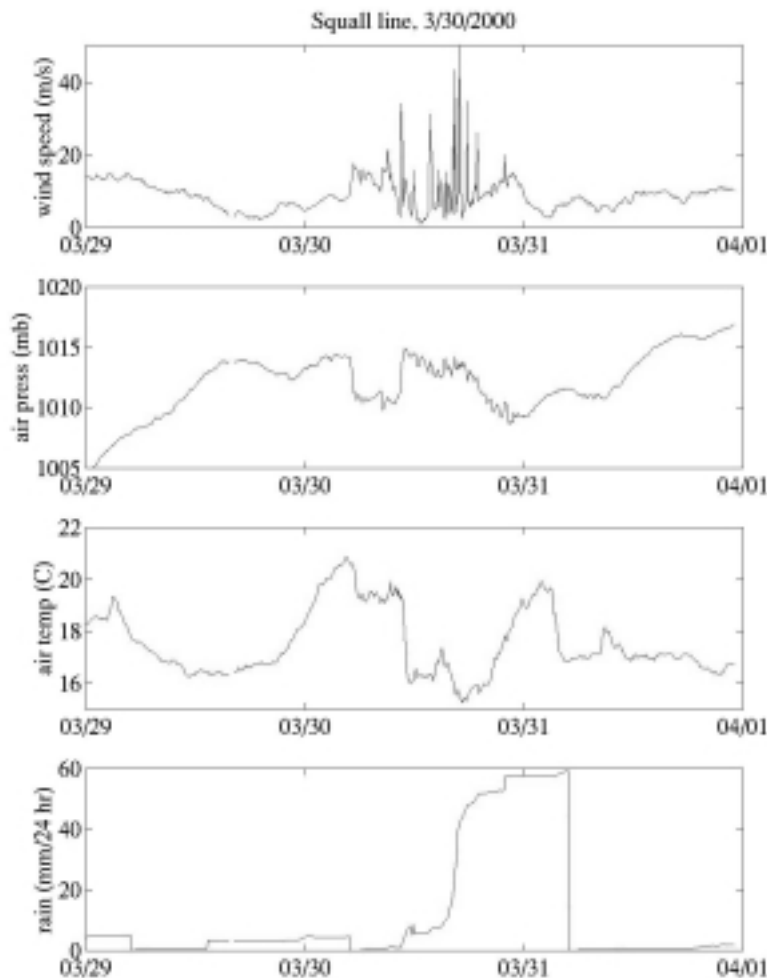


Figure 5. Six-minute average wind speed, air pressure, air temperature and 24-hour cumulative rainfall during an extreme wind event. The rapid drop in air temperature corresponds to an increase in air pressure that is followed by high-frequency fluctuations. A downpour and wildly variable winds are also signatures of the events, which have been observed more than a dozen times in the last year.

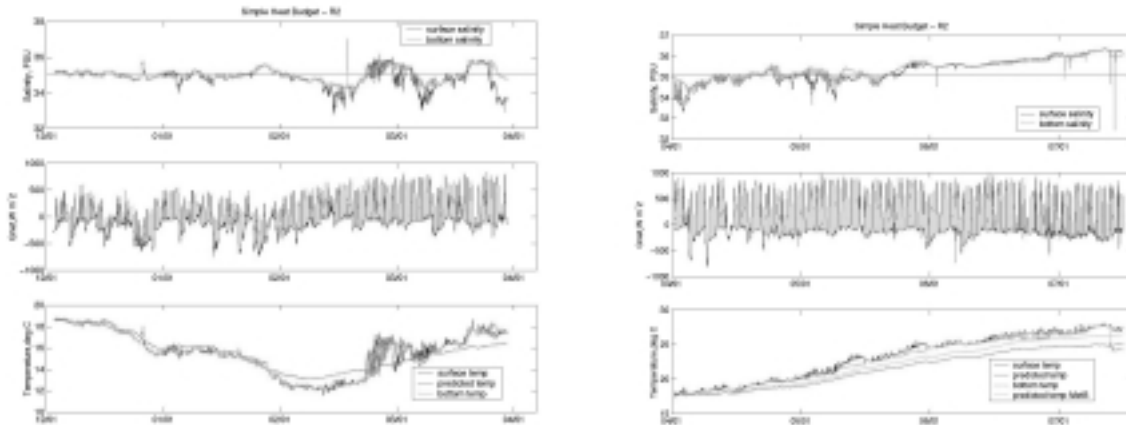


Figure 6. Near surface and near bottom salinity (top), net heat flux (middle) and measured and predicted ocean temperature (bottom) at R2, for December 1999-April 2000 (left) and April – July 2000 (right). The ocean temperature predicted from integrating the heat flux (red line) is consistent with the observations in the winter when salinities are near 35.1 psu (top panel, red line). Departures from the prediction correlate with salinity variations and imply cross-shelf advection. In spring and summer, using atmospheric temperature and humidity from 50 m (bottom right panel, red) underpredicts ocean warmer, whereas use of measurements from 10 m (cyan) significantly improves the prediction.

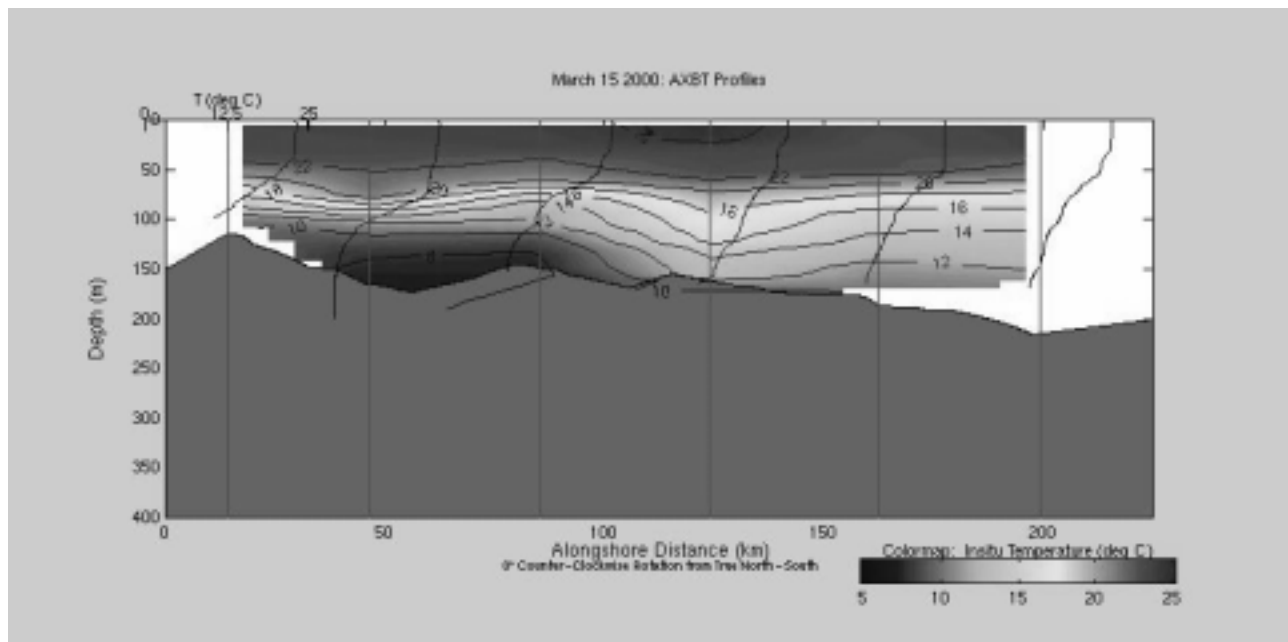


Figure 7. An AXBT section from south to north along the shelf break offshore of the tower reveals a meander pushing onto the shelf near 120 km. The alongshore propagation of the meander was apparent in the repeated aerial surveys.

observations that indicate the resuspension of fine particles from the sand sediments of the shelf during storms (Nelson et al. 1999). Similar wave measurements from other depths (towers) on the shelf should help clarify this issue.

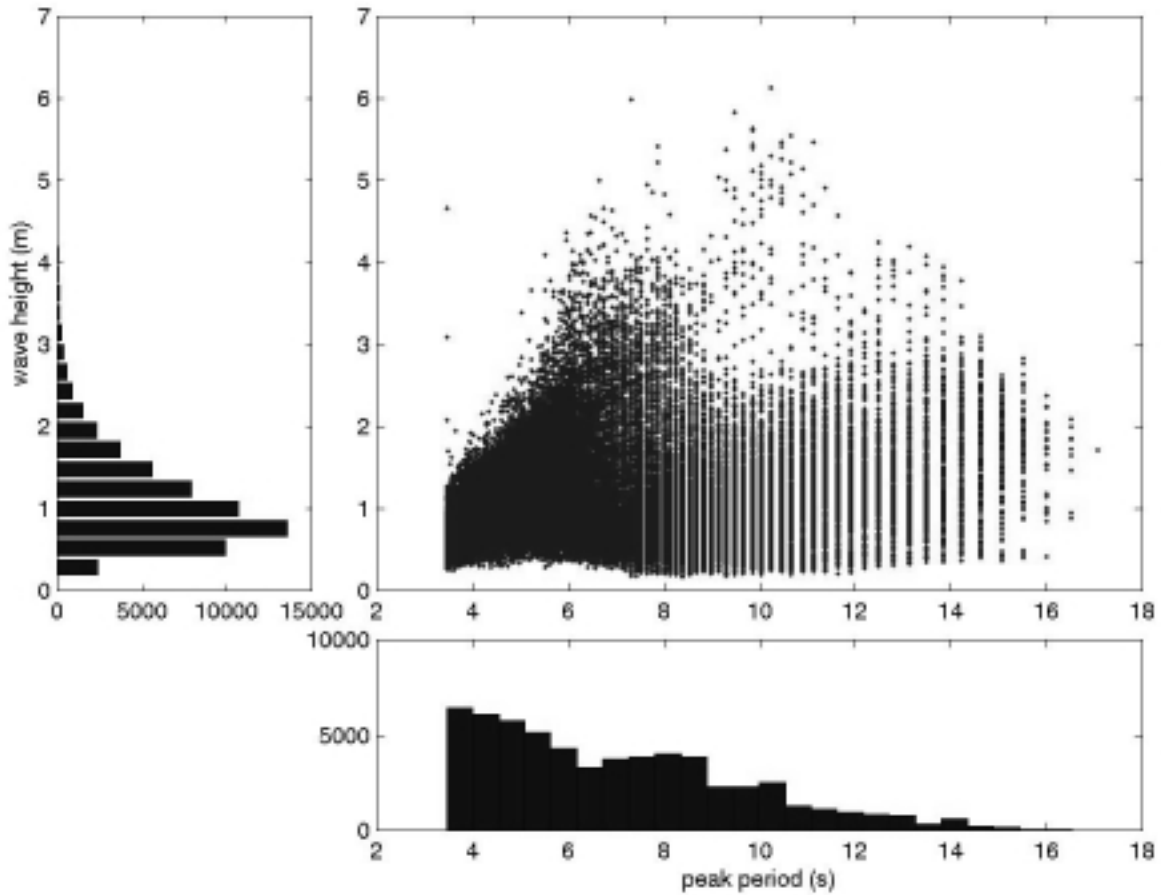


Figure 9. *The distribution of surface wave significant wave heights and peak periods between July 1999 and July 2000. Typical wave heights are 0.5 to 1.5 m, and several periods are preferred (4, 8 and 10 seconds). The joint distribution envelope forms a triangle. The left side of the envelope follows the maximum growth rate curve to roughly 10 second periods. The right side of the envelope is apparently set by the shoaling on the shelf. The result is that maximum wave heights on the shelf occur between 8-12 seconds.*

A diurnal variation in wave heights has been observed during times of weak atmospheric forcing. When the sea breeze, which extends at least 50 km offshore to R2, opposes the tidal currents, wave heights exhibit a 0.5 m daily variation.

Tides are dominated by the M_2 tidal constituent (79 cm), with only minor contributions from N_2 (18 cm), S_2 (14 cm), and K_1 (10 cm). Subtidal water level varies over 0.5 m at a range of time scales, from days (especially associated with the passage of hurricanes) to weeks and months (Figure 10). The low frequency water level fluctuations display some correlation with low-frequency temperature and salinity variability. These T/S variations are not obviously related to

meteorological forcing and may result from cross-shelf pressure gradient variability associated with movement of the axis of the Gulf Stream.

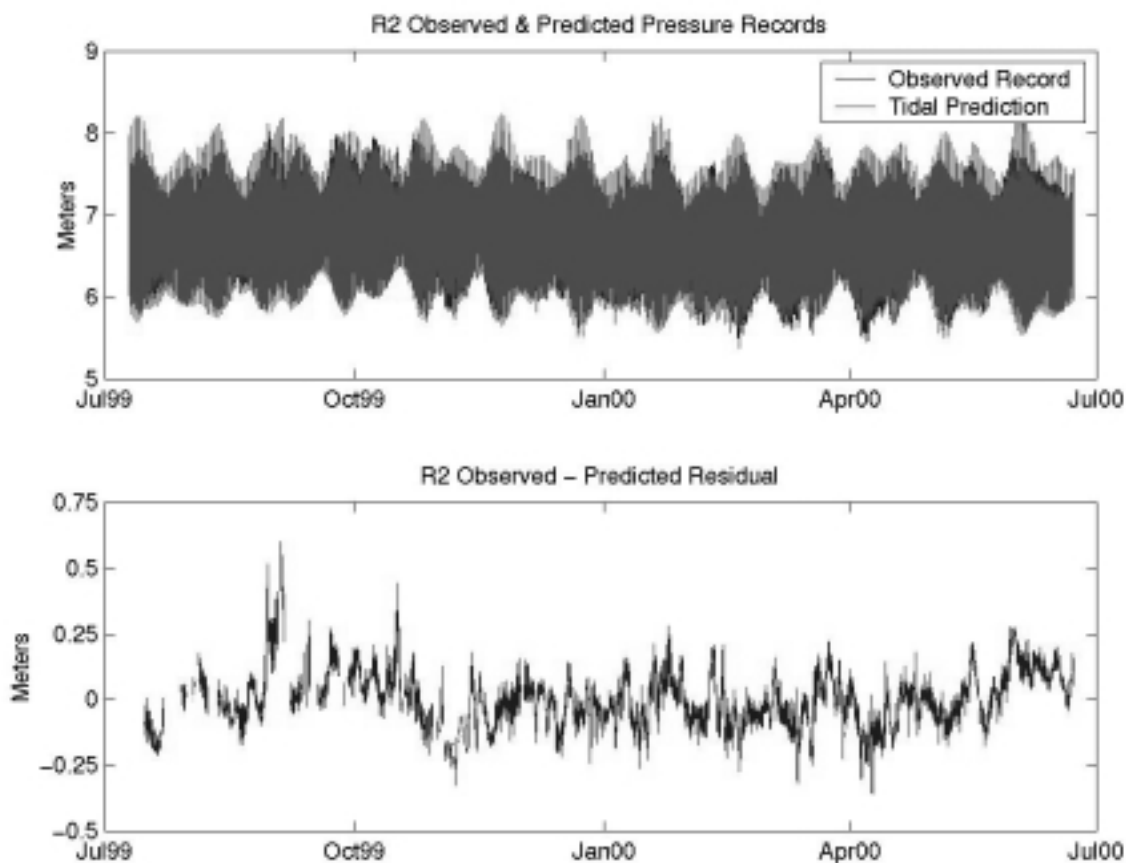


Figure 10. Observed and predicted water levels at R2. The unusually weak S_2 tides on the shelf produce a maximum spring tide once a month, especially during winter months. The residual water level displays a remarkable amount of variability over a range of time scales. The influence of Hurricane Floyd produced the high in Sept. 1999.

Temperature and salinity time series

Seabird MicroCat conductivity-temperature-pressure sensors are deployed at 4 m and 23 m mean depths in 28 m deep water at R2. The packages are attached to carriages suspended on a trolley system that can be recovered for servicing or maintenance from the tower without a ship or divers. Optical sensors on the carriages require pumping, so the conductivity sensor is also pumped to ensure it is well flushed. One minute averages are collected every 6 minutes.

The seasonal cycle is apparent in the ocean temperature measurements, which reached a minimum in mid-February 2000 (see Figure 6). Salinities average 35.2 psu but show considerable variability, from 33 to greater than 36 psu. Low salinities are associated with movement of nearshore water to mid-shelf, whereas high salinities are due to intrusions of Gulf Stream water on to the shelf. A T/S

diagram illustrates the variety of water masses that have been observed at R2, and implies there is strong mixing occurring on the shelf (Figure 11).

Stratification has been intermittent since January. The strongest stratification has been associated with arrival of nearshore waters at mid-shelf in winter and early spring and with Gulf Stream intrusions in the summer (Figure 12). Peak values exceed 10 cycles per hour ($>4 \times 10^{-4} \text{ 1/s}^2$) and persist for several weeks. Sustained stratification in mid-winter came as surprise; previous studies had suggested that well-mixed conditions dominate during wintertime (Atkinson et al., 1983).

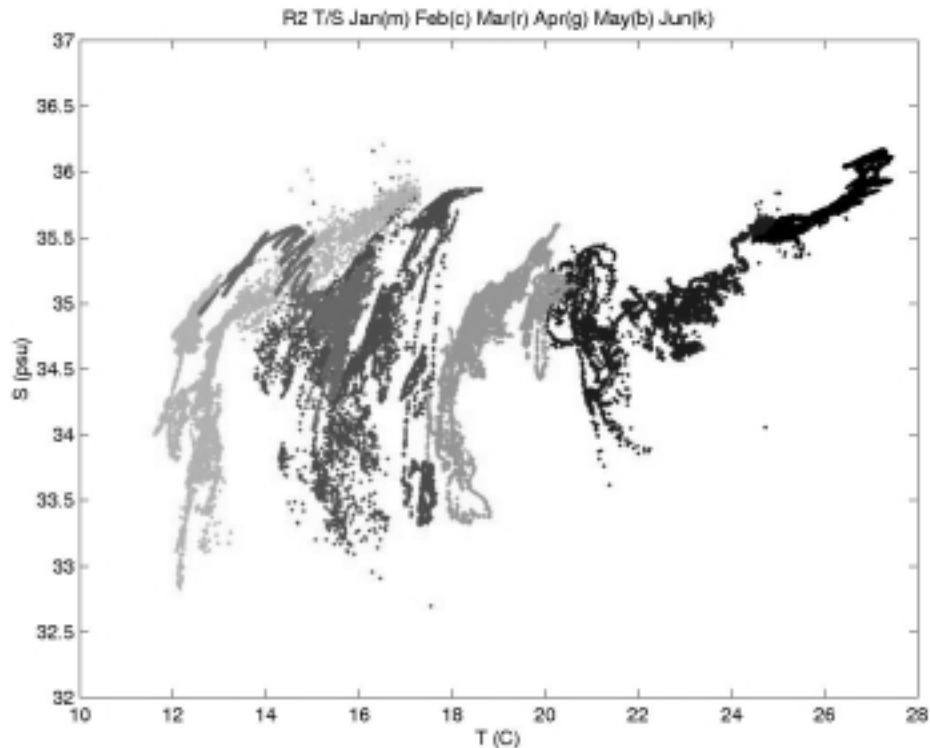


Figure 11. Temperature/salinity plot of observations from the near-surface package at R2. The different colors represent different months between January and June 2000. Minimum temperatures in February (cyan) are accompanied by the maximum salinity variability. The range of salinities observed narrows significantly in May.

Since mid-April temperature has been measured at towers R2 and M2, providing a measure of the cross-shelf thermal gradient. Over the winter and until mid-May the inner shelf was cooler than offshore, but this gradient changed sign in mid-May, and rapidly increased through June. Thermal wind arguments suggest this change in sign should be accompanied by a change in mean flow direction along the shelf. In July, several large temperature reversals occur, associated with (bottom-trapped) Gulf Stream intrusions onto the shelf.

In-water bio-optical measurements

In-water optical sensors has been deployed at the R2 tower, measuring: (1) the flux of photosynthetically available radiation (PAR) at a mean depth of 23 m (LI-COR LI-192SA sensor); (2) stimulated chlorophyll fluorescence (WETLabs Wetstar fluorometer); and (3) the fluorescence of colored dissolved organic matter (CDOM, WETLabs FlashLamp fluorometer). The fluorometers are included in both the near-surface and near-bottom packages at R2. Additional optical instruments will be deployed in the next phases of the project, including sensors for measurements of beam attenuation and attenuation/absorption (WetLabs beam transmissometer, ac-9).

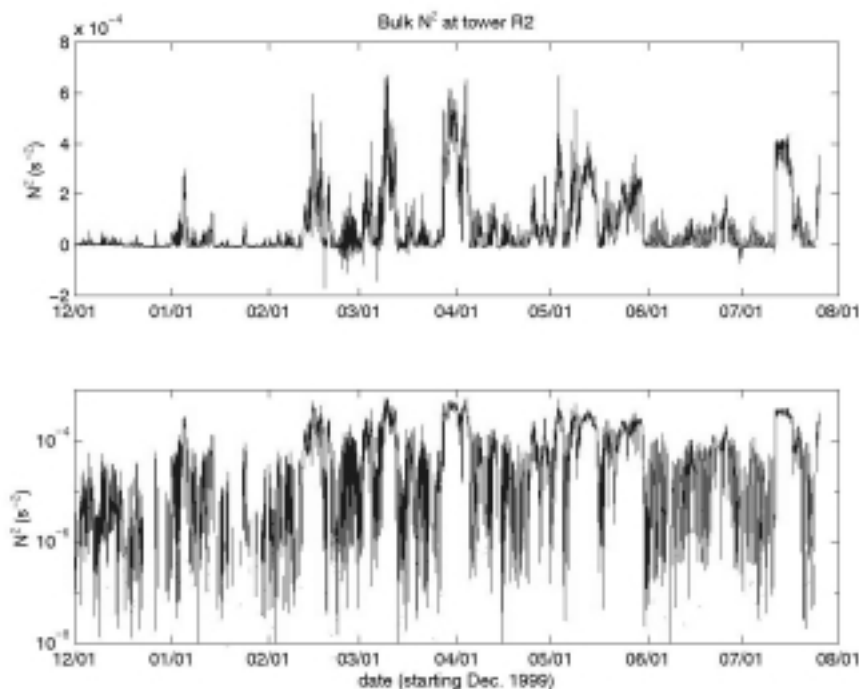


Figure 12. Stratification at R2 between December 1999 and August 2000 on a linear (top) and logarithmic scale (bottom). Peak values occurred in later winter and exceed $5 \times 10^{-4} \text{ s}^{-2}$ (12 cycles per hour) and were associated with fresh water outflow from the coast. Episodes of stratification in July were associated with intrusions of Gulf Stream-derived waters.

A key consideration for the long-term *in situ* deployment of optical systems is bio-fouling. Since the present instruments represent three different optical configurations, several anti-fouling strategies have been employed and evaluated.

The irradiance collector plate of the PAR sensor is a teflon disk on one end of a cylindrical sensor body. To inhibit fouling, a TBT-impregnated ring (Oceanographic Systems, West Palm Beach, FL) was mounted around the PAR sensor. Based on measurements before and after cleaning, this system has been effective for periods of up to 2 months (fall-spring). However, since recharging the TBT-rings represents a significant recurring cost for multiple tower deployments, we also

intend to evaluate a mechanical copper-shutter system for irradiance and radiance collectors if sufficient power is available.

The chlorophyll fluorometer is a flow-through sensor that is plumbed in-line between the conductivity sensor (which has a TBT fitted intake) and pump. Instrument stability has been evaluated with a fluorescence reference (coproporphyrin) at servicing intervals and has proven to be quite good. Initially a bromine canister system was installed for in-line anti-fouling, but this was not effective and fouling resulted in an upward trend in the fluorescence signal between servicing intervals. The bromine canister was removed and copper tubing was installed in-line on either side of the fluorometer (on the recommendation of Tom Dickey). This has been effective in preventing fouling for the late winter through spring period. Currently we see little or no offset in the signal following monthly servicing.

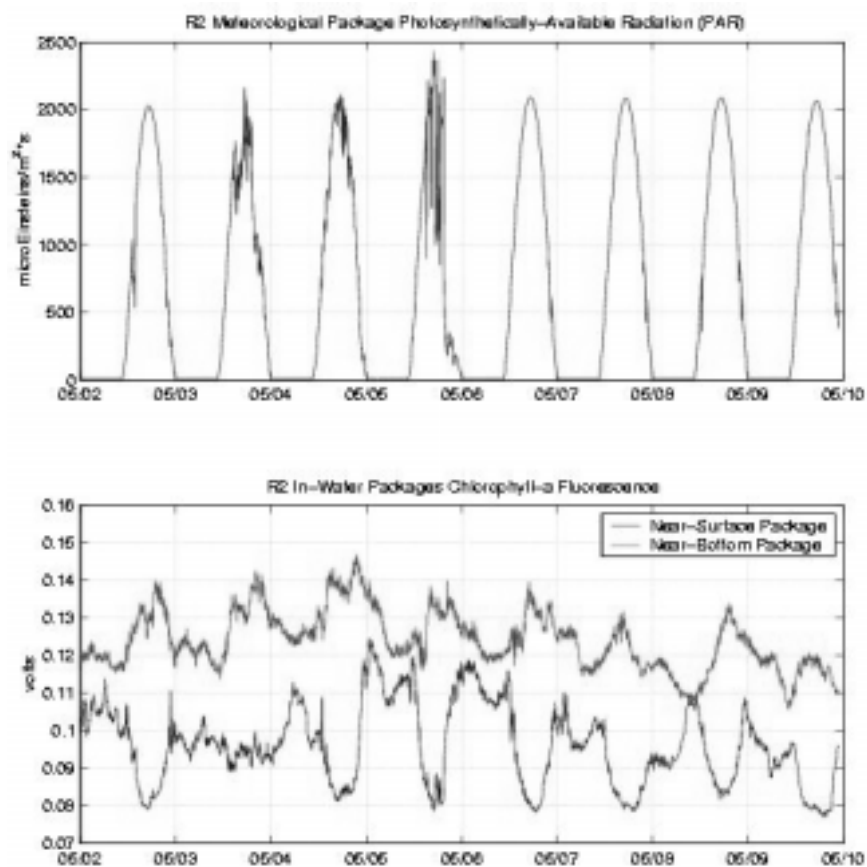


Figure 13. Surface visible irradiance at the R2 tower from May 2000 and diurnal fluctuations in stimulated chlorophyll fluorescence from the two in-water packages (about 3.5 m and 23 m). Upper panel: photosynthetically available radiation (PAR, $\mu\text{mol photons m}^{-2} \text{s}^{-1}$). Lower panel: chlorophyll fluorescence (raw data output, in volts).

The CDOM fluorometer has an open optical configuration with external excitation and emission windows and has been most affected by bio-fouling. A TBT-impregnated block (Oceanographic Systems) has provided anti-fouling protection for the excitation/emission windows, but bio-fouling of adjacent surfaces has interfered with the CDOM signal. Hydroid colonization and growth has

been rapid in the spring, and, as they elongate, the hydroids can extend into the open optical path, causing a spiking of the output signal. There has also been an accumulation of debris from tube-building amphipods in the instrument housing around the optical windows that may also contribute to spiking of the fluorescence signal, as may the amphipods themselves as they move about on the exposed surfaces. Enclosure of the optical end of the instrument with a copper mesh has not completely eliminated bio-fouling and the intermittent signal spiking, but appears to have stabilized the baseline signal. A despiking routine implemented for the processing of the CDOM fluorescence data appears to be effective.

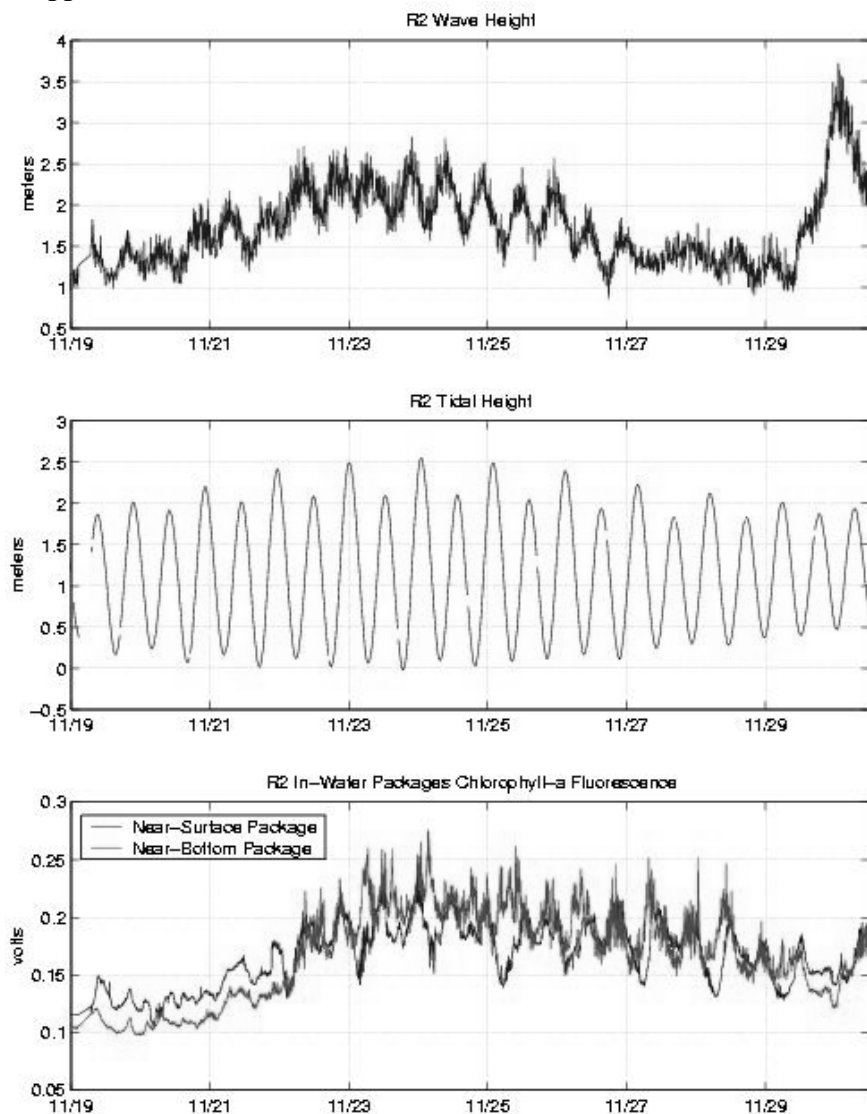


Figure 14. A fall storm event at tower R2 (November, 1999). Surface wave heights (upper panel) and tidal height (middle panel) derived from the pressure sensor record, and near-surface and near-bottom stimulated chlorophyll fluorescence (lower panel). Strong north to north-easterly winds generated surface waves in excess of 2 m height during a spring tide period. In-water PAR measured at the bottom package (not illustrated) was reduced to near-zero values from 11/22 through 11/30. The increase in chlorophyll fluorescence during the storm event may be due to suspension of benthic diatoms from the sand sediments (Nelson et al. 1999).

Results from bio-optical time series

In combination with the above-water PAR sensor (Met package), the in-water PAR sensor provides information on the variability of attenuation of visible light in the water column and thus the availability of light for photosynthesis. The euphotic zone often reaches the sediment surface across much of the SAB mid-shelf region, and an abundant benthic diatom flora is found in these sand sediments (Nelson et al. 1999). Aerial primary productivity by the benthic community can match or exceed that of the overlying water column, and appears to be strongly light-dependent (Jahnke et al. 2000). The R2 time series has thus provided a continuous record of above- and in-water PAR and will provide a continuous *in situ* record for comparison to PAR products derived from satellite observations (SeaWiFS, MODIS).

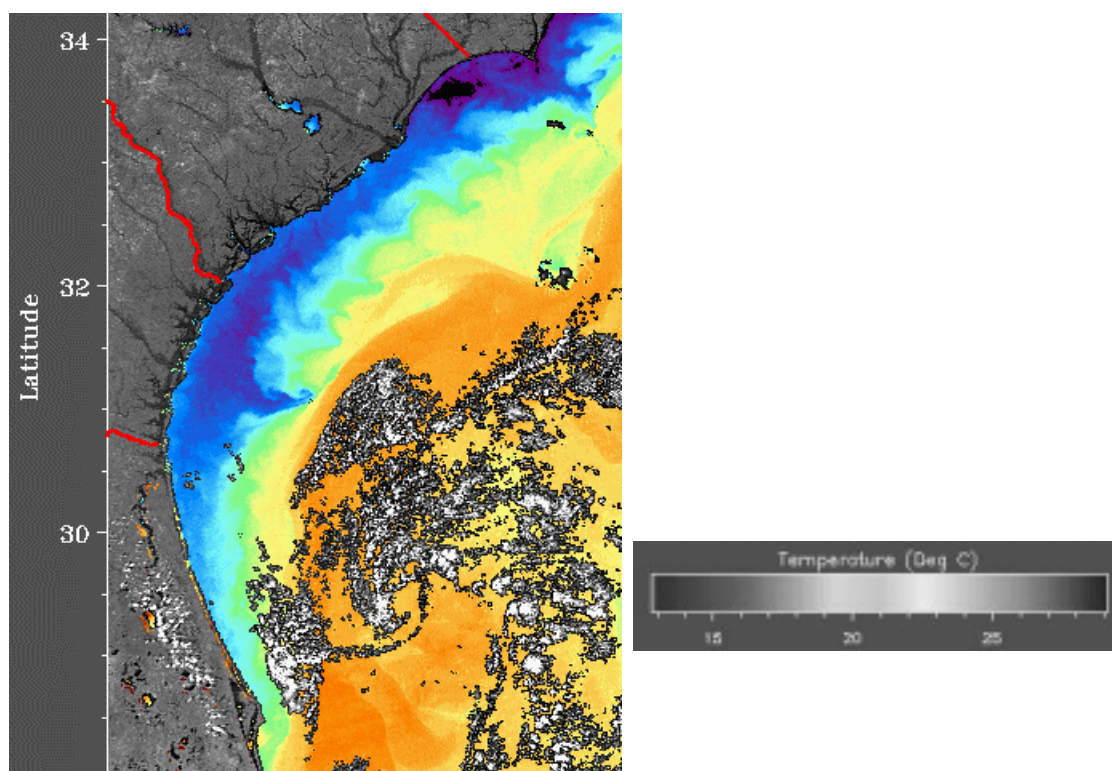


Figure 15. AVHRR SST imagery for 29 February, 2000. Produced by the Johns Hopkins University Applied Ocean Physics Laboratory. In early Feb. the large cold plume feature was further north (off the GA-SC border) and extended to the Gulf Stream.

Chlorophyll fluorometers on the surface and bottom packages provide a sensitive indicator of the chlorophyll concentration in the water column. However, stimulated chlorophyll fluorescence is a physiological variable and is thus affected by the physiological status and recent light history of the phytoplankton population. Under clear sky conditions, the signal from the near-surface instrument typically shows a mid-day depression of stimulated chlorophyll by some 10-20% from the night levels (Figure 13), likely due to photoadaptive/photoprotective responses in the surface phytoplankton. In contrast, under the lower light conditions sampled by the near-bottom package, chlorophyll fluorescence often increases in the afternoon, which result from a combination of daytime increase in chlorophyll and physiological adjustments by the phytoplankton. A distinct

increase in chlorophyll fluorescence, along with increased attenuation of PAR, has also been observed during wind/surface wave events (Fig. 14), suggesting that benthic diatoms and other fine particles have been resuspended from the sediments. Episodic mobilization of organic particles from the sediments and subsequent advective transport could represent a significant mechanism of cross-shelf biogeochemical exchange in the SAB, particularly during the fall transition period.

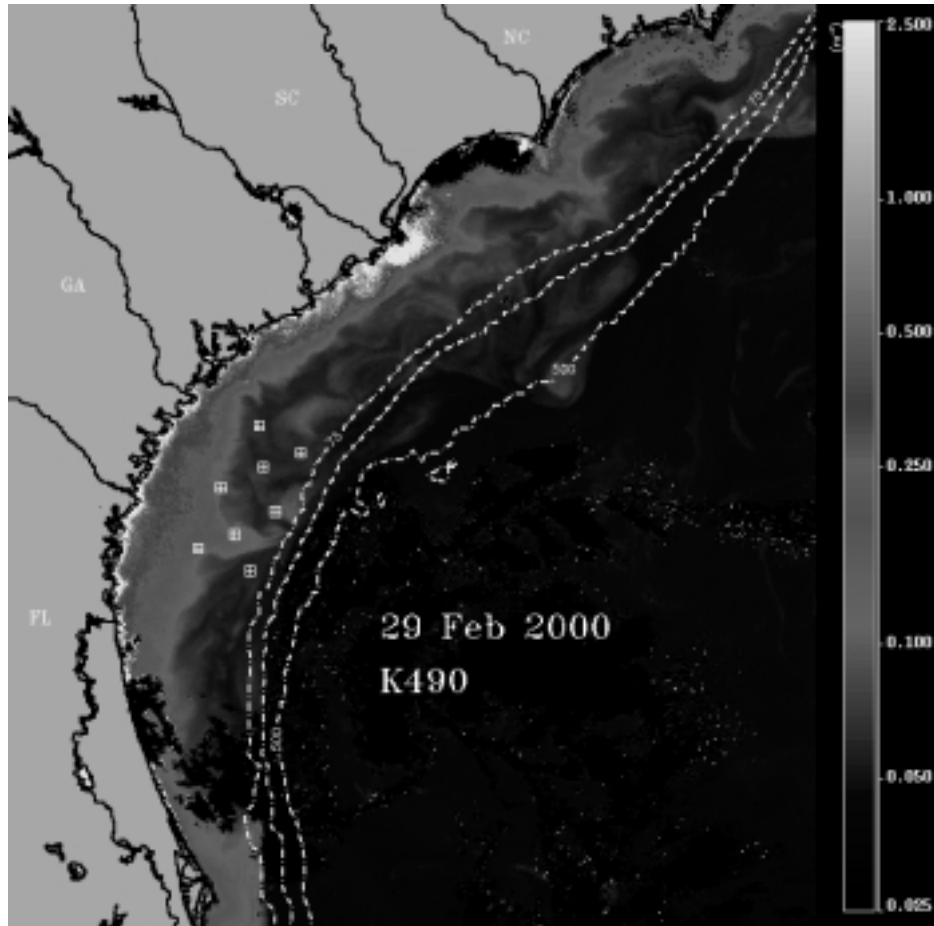


Figure 16. SeaWiFS K490 imagery from 29 February, 2000. The color scale is from 0.025 m^{-1} to 2.5 m^{-1} (log scale). The turbid coastal band is typical. The positions of the TACTS towers and the 75, 200 and 500 m isobaths are indicated.

Another important biogeochemical question for the SAB shelf region is the fate of terrigenous organic matter that is delivered to the coastal zone in the form of dissolved organic matter (DOM) from the rivers and estuarine system. There is a strong optical signal associated with the DOM input, since colored components of DOM absorb strongly at shorter visible and near-UV wavelengths and fluoresce under UV excitation. The fluorescence of CDOM provides a sensitive indicator of the relative concentration of CDOM in shelf waters and can serve as an optical tracer of lower salinity water on the shelf. During periods which combine high freshwater discharge with offshore (upwelling favorable) wind stress, lower salinity surface features detach from the coastal frontal region and extend across the mid-shelf (e.g., Blanton 1981; Chen et al, 1999). Under these conditions, CDOM can dominate the total absorption in the violet-to-blue spectral regions across the SAB mid-shelf (Nelson and Guarda, 1995). Winter-spring satellite SST and SeaWiFS ocean

color imagery has consistently shown the formation of plume-like features extending from the Georgia coast through the SABSOON area (Figures 15 and 16). Thus, the TACTS towers appear to be well situated for *in situ* observations of seasonal cross-shelf exchange events.

The time series of CDOM fluorescence shows an inverse relationship between CDOM fluorescence and salinity fluctuations in the short term (higher with lower salinity). However, this relationship is not consistent over longer periods (weeks to months), reflecting both the advection of different water masses past the R2 tower and the likely degradation of a portion of the CDOM pool with time on the shelf. For example, there has been a pronounced decline in the CDOM fluorescence baseline (de-spiked) signal from winter through spring, corresponding with increasing salinity. Since rainfall in the winter-spring period of 1999-2000 was fairly low, there was less freshwater discharge to the shelf. Thus the seasonal “recharge” of the CDOM signal on the shelf has also been less than may be typical of the winter-spring period. Also, as lower salinity water is transported seaward from the coastal zone, particles settle out and the water becomes much clearer. Thus in the mid-shelf region, the relatively refractory DOM would be subject to the combined effects of photochemical and microbial processes (Moran and Zepp, 1997), and thus the decline of CDOM fluorescence with time could also indicate the remineralization and utilization of terrestrially derived organic matter on the shelf.

Currents

An upward-looking, bottom-mounted RDI ADCP has been deployed 200 m from tower M2 since mid-April 2000. Cabling between the ADCP and tower provides power and communications. The 300 kHz unit outputs a 150 ping averaged profiles every six minutes with 1 m vertical resolution. Tidal currents explain 75% of the velocity variance, the depth-averaged M2 tidal current having a major axis amplitude of 28 cm/s and a minor axis amplitude of 10 cm/s. The observations capture the polarization of the tidal and subtidal barotropic flows on the shelf (Figure 17) where depth-averaged tidal currents are largely rectilinear and directed across isobaths (e.g. Pietrafesa et al., 1985) and depth-averaged subtidal (wind-forced) flows are principally along isobaths (e.g. Lee et al., 1985).

Subtidal flows follow isobaths and the seasonal winds. Currents have been generally northeastward since installation in mid-April (Figure 18), associated with the southwesterlies common at this time of year, but have been southwestward since early September. A first-baroclinic-mode-like flow dominates the subtidal cross-shelf circulation, and produces on average an estuarine-like cross-shelf transport (Figure 18). This is similar to the cross-shelf flow observed further inshore (Blanton, 1996) and suggests coastal zone influence extends more the 50 km offshore.

Fisheries Life History and Behavior

The South Carolina Marine Resources Division (MRD) (in particular Charlie Barans and Jack McGovern of the Marine Resources Research Institute and David Schmidt with Smartech) has developed a system for transmitting images of marine fish assemblages off Georgia to computers in offices of scientists and homes of the general public. The underwater TV camera system on the bottom offshore allows study of fishes throughout the year without the costly trips to a research site in inclement weather. Images are transmitted via the Navy microwave system to shore, and then to user groups by the World Wide Web and, potentially, to the South Carolina Educational Television

Network (SC ETV). This "remote sensing" research required the application of image capturing and transmission software and hardware. The resulting capability should enhance fisheries biologists' understanding of fish movements within the region.

Often important fish behaviors, such as the feeding or spawning events in which the biologist is most interested, occur relatively rarely. Observation of rare events often requires long-term observations, which are difficult to obtain under natural conditions. Spawning in many reef fish off the southeastern US occurs during late winter or early spring when frequent storms can make sea surface transportation unpleasant and often dangerous to both personnel and equipment.

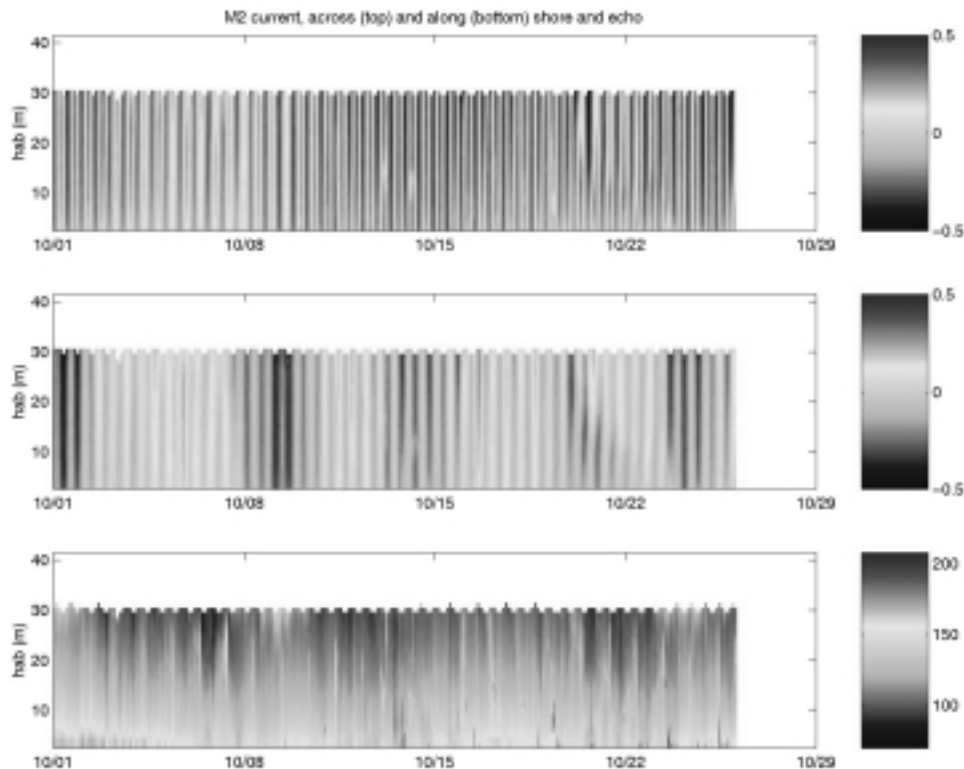


Figure 17. Across-shelf (top) along-shelf (middle) currents, in m/s, as a function of depth and time reveal a remarkable polarization of tidal frequency and subtidal frequency motion on the shelf. Echo intensity (bottom) is characterized by a pronounced diurnal migration that culminates in a pre-dawn maximum that is at times strong enough to impact the current observations. Near-surface echo intensity maxima correspond to storm events and are likely the result of bubble plumes.

The small black and white security cameras (PC-23C) that were deployed for the initial fisheries video trials have low light capabilities (to 0.04 lux) and relatively low resolution (460 lines). Camera lenses of 8 mm allowed a 12 degree angle of view and the sea bed was in view at about 13.7 m from the camera. Daily observations (~65) have been collected between 1230 and 2130 GMT. Still images ~15 KB (jpg) are recorded and logged at ten minute intervals while 10 sec. video clips ~400 KB (avi) are recorded on the hour from camera No. 5. Images are downloaded from the remote computer to the laboratory computer for fish counts and long-term data storage.

Only camera No. 5, with an 8 mm lens, was directed at reef structure with any reef fish activity. Quantitative counts of fishes by species can be conducted during the standardized temporal sampling, although this can be complicated periodically by low visibility.

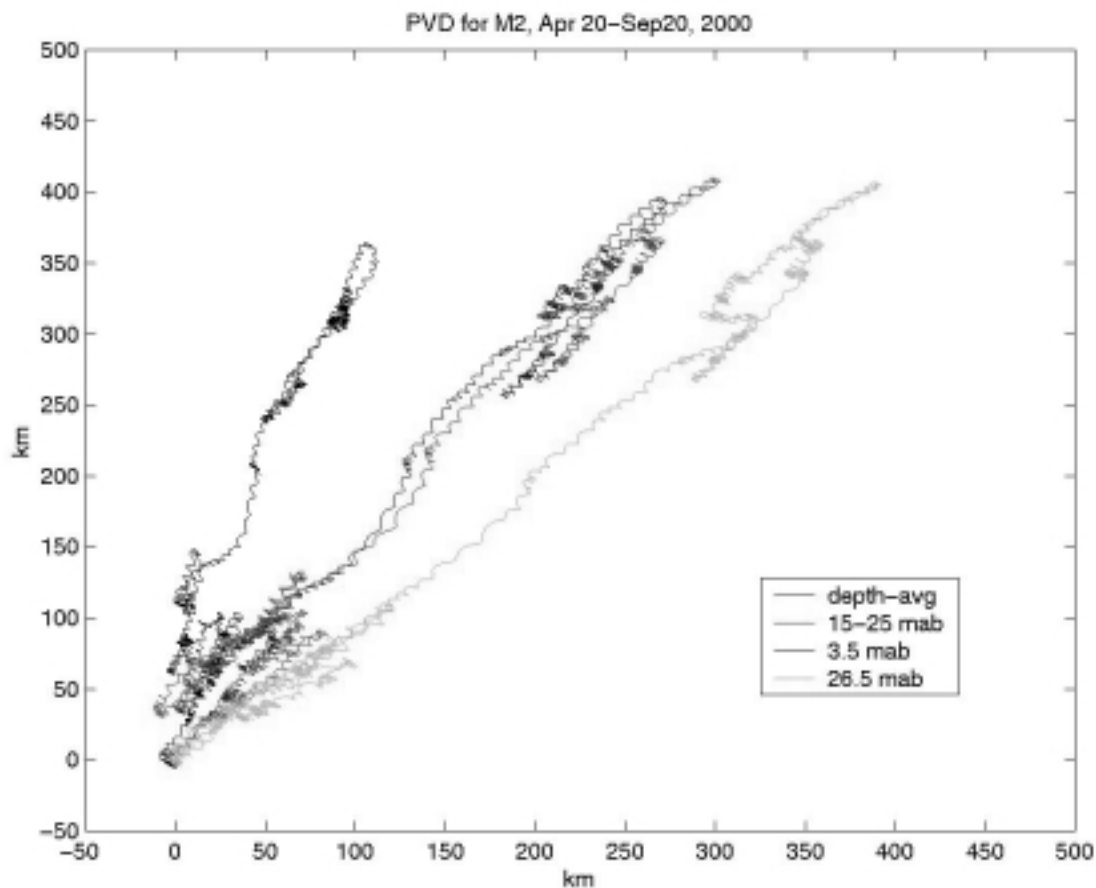


Figure 18. Progressive vector diagram of current observations from ADCP observations at M2 between April and September 2000. Depth-averaged currents (blue) follow the local isobaths (oriented NE-SW). Near-bottom currents (black) have an onshore component and near-surface (cyan) currents a distinct offshore component.

Although resident predators must significantly reduce recruitment of many species, the influence of large stochastic predation events appear to be formidable influences on mortality and survival of small and juvenile reef fishes. The two most important large scale predation events seen in 1999–2000 were the temporary appearances of large numbers of migrating loons (diving birds) and the mid-winter populations of ctenophores (comb jellies) and cnidarians (jellyfish). The loons were observed to visually select fish prey in and near the structural units within a meter of the bottom. Also, the large populations of ctenophores and/or jellyfish in winter corresponded to the temporary residence of a *Mola mola* (ocean sunfish) and a relatively large population of adult Atlantic spadefish; both species are known to feed on jellyfish. Resident predators at the site include black sea bass, greater barracuda and, possibly, juveniles of some of the less frequently observed transient species. The importance of predator-prey relationships was inferred from general observations of the relatively simultaneous arrival of juvenile baitfish and some of the higher level

predators in the early spring. The infrequent appearance of higher level predatory fish at the small artificial reef site suggests that many of the larger species are "passing through" the site while looking for feeding opportunities within a larger feeding range. Species that may move back and forth between other habitats within their large hunting range and were observed at the site include large adults of: loggerhead turtles, sand bar sharks, American red snapper, gag grouper and scamp grouper.

Observations from the SABSOON fish research site can contribute significantly to the understanding of short-term and long-term temporal changes in an offshore reef fish population. Permanent installations of underwater TV systems have the advantage of non-obtrusive observations of fish interactions without behavioral changes that can occur in the presence of divers (ranging to complete avoidance). Also, seasonal observations by divers are severely limited during seasons of high seas often including both winter and spring when migration and spawning activities occur.

Assimilation of Tower Data to Model the SABSOON Coastal Ocean

The NOPP-funded project "*Limited-Area Operational Coastal Ocean Models: Assimilation of Observations from Fixed Platforms on the Continental Shelf and Far-field Forcing from Open Ocean Models*" (Lynch et al, PIs; proposal available from <http://www-nml.dartmouth.edu/circmods/SABSOON/proposal/N99.html>) will develop an operational, data assimilative, coastal ocean model of the South Atlantic Bight (SAB). The SAB was chosen to take advantage of the unique observational data that has recently become available from the South Atlantic Bight Synoptic Offshore Network (SABSOON). It is clear that realistic modeling of circulation, hydrography and biochemical processes in coastal oceans must rely on assimilation of "external" data. Thus the application portion of this work will focus on developing an understanding of the effectiveness of assimilating various types of data into a coastal ocean model. As such, the SABSOON towers provide a unique source of physical and biological observational data (including water level, air-sea fluxes and vertical profiles of velocity, hydrography and several biochemical parameters) in the SAB. Other important observational data sources include river discharge, water levels from NOAA coastal sea level stations and satellite derived maps of SST, chlorophyll and perhaps sea surface height. In addition, the SABSOON program includes several aircraft surveys (AXBT) of the SABSOON region that can be used to provide a detailed set of initial conditions for the modeling efforts.

Sensitivity to input SABSOON tower data

The sensitivity to data available from the towers is illustrated by a sequence of numerical experiments that explores the level of domain-wide "truth" recovered as an increasing amount of data becomes available from activating more towers. Herein the "truth" is provided by a "forward" model solution (forced by the M2 tide and a steady wind to the south). The velocity of the forward solution is then sampled at the towers for a period of 5 days, effectively simulating measurements that would be obtained by ADCPs fixed at the towers. The experiments that follow examine the sensitivity of the recovered solution to velocity data collected at one tower, three towers, and all 8 towers. Figure 19 shows the finite element computational domain and the tower locations.

The “true” M2 elevation solution is shown in Figure 20a. Velocity data from this solution is assimilated into a model that inverts for boundary conditions that, in a weighted least square sense at selected frequencies – in this case the M2 and zero-frequencies, best reproduce the input/observed velocity record at the particular tower locations. The difference between “truth” and inverted solutions for assimilation of data from tower R2 is shown in Figure 20b. Similarly, assimilation of data from three towers (R2, R1M1 and R6M2) results in the differences shown in Figure 20c, and finally the inclusion of all eight towers results in the differences shown in Figure 20d. The improvement in the overall solution is apparent. With only R2, the maximum error in the domain is approximately 0.5 m, with the southern extreme of the domain exhibiting errors greater than 30 cm. Note that the elevation error in the vicinity of R2 itself is less than 10 cm. The inclusion of R1M1 and R6M2 decreases the maximum error as well as improving the solution domain-wide. Similar improvements are obtained by the inclusion of all 8 towers.

The sensitivity of the zero-frequency solution follows the same pattern (Figure 21). The “true” steady state elevation is shown in Figure 21a, and the difference between true and inverted solutions for one, three and eight towers are shown in Figures 21b, 21c and 21d, respectively. Within the domain, the improvement in the solution as data from additional towers is included is more apparent in the middle and northern regions of the domain, than in the southern extreme. Note that the southern region is “downstream” of the tower array (and the data) as defined by the sense of a propagating shelf/Kelvin wave. Hence the solution along the southern boundary does not affect the upstream portion of the solution, i.e., it is relatively unconstrained by the tower data and thus it is not surprising that the errors are larger along this portion of the domain.

It is apparent from these results that the full implementation of the SABSOON tower array is desirable. Even for these relatively simple and large scale responses to tidal and wind forcing, the inclusion of additional towers (data) clearly improves the modeling capabilities. As smaller scales (in space and time) are considered, we expect the additional data provided by the towers to be even more critical to our abilities to study effects of Gulf Stream intrusions, wind and storm events and their impact on biogeochemical processes.

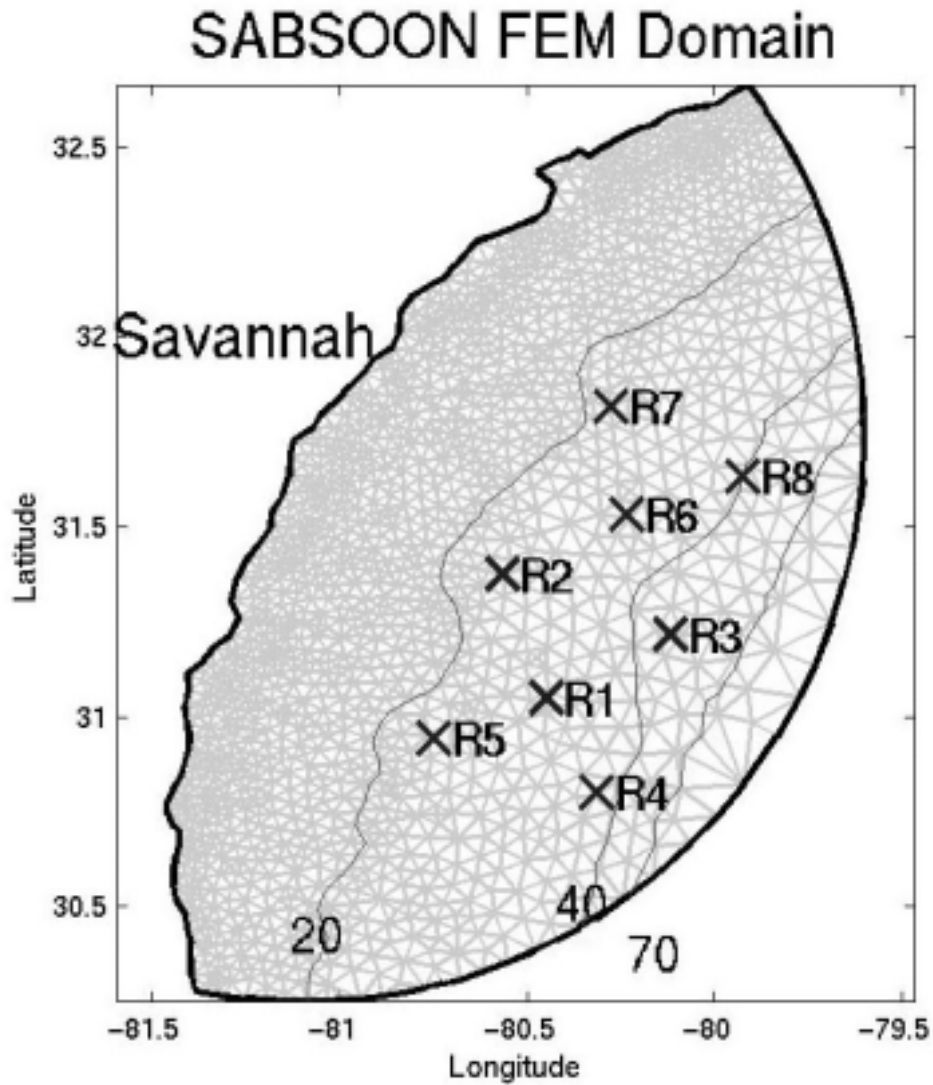


Figure 19. Computational domain, 20, 40 and 70m bathymetric contours, and the location of the SASBOON towers. The finite element mesh has on the order of 1700 nodes and 3200 elements. Grid resolution ranges from 2 to 15 km.

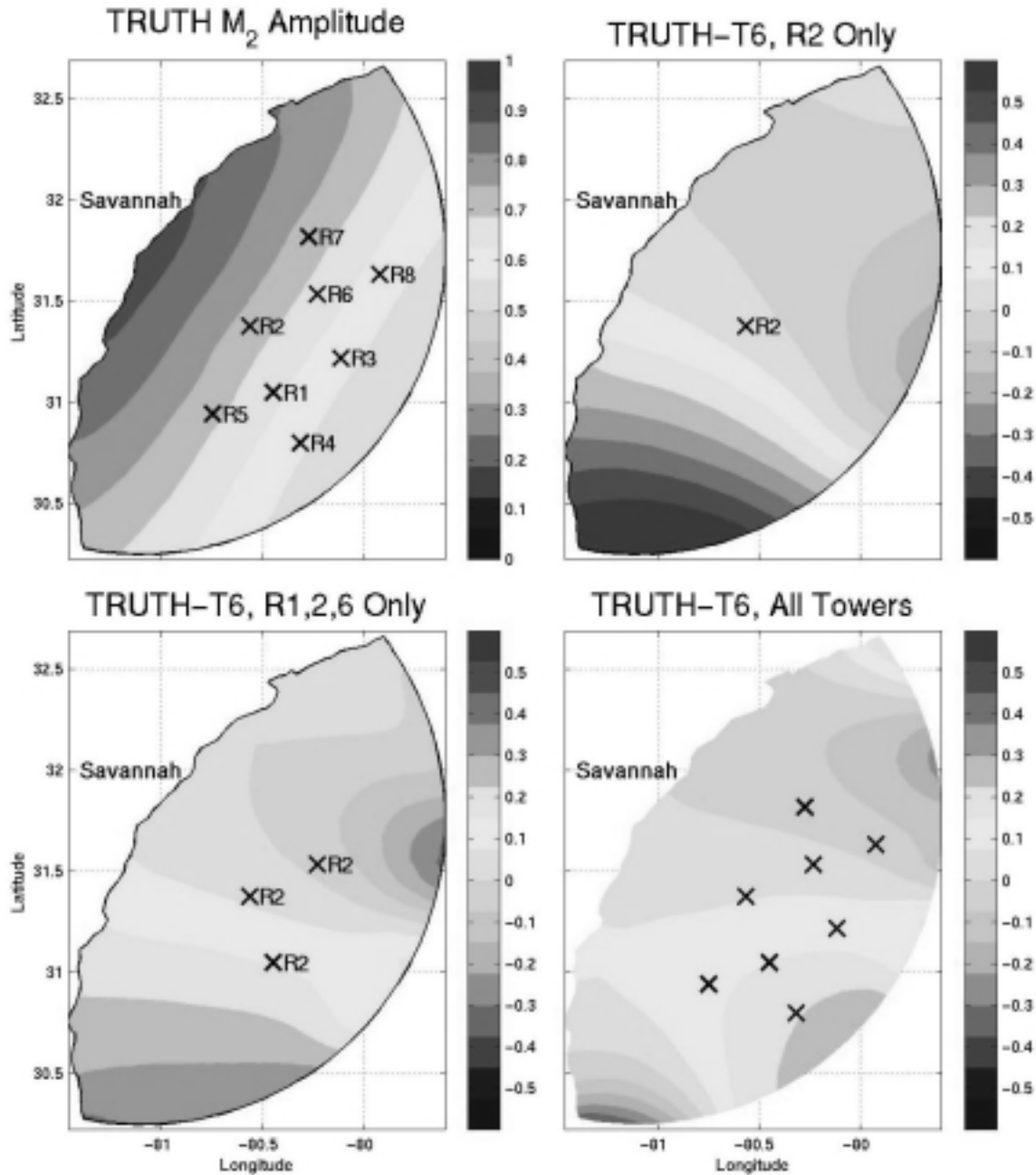


Figure 20. M_2 tidal amplitude. True solution, top left (a); true minus solution computed with one tower, top right (b); true minus solution computed with three towers, bottom left (c); and true minus solution computed with eight towers, bottom right (d). Note that the scale of the true solution is different from the difference between true and computed.

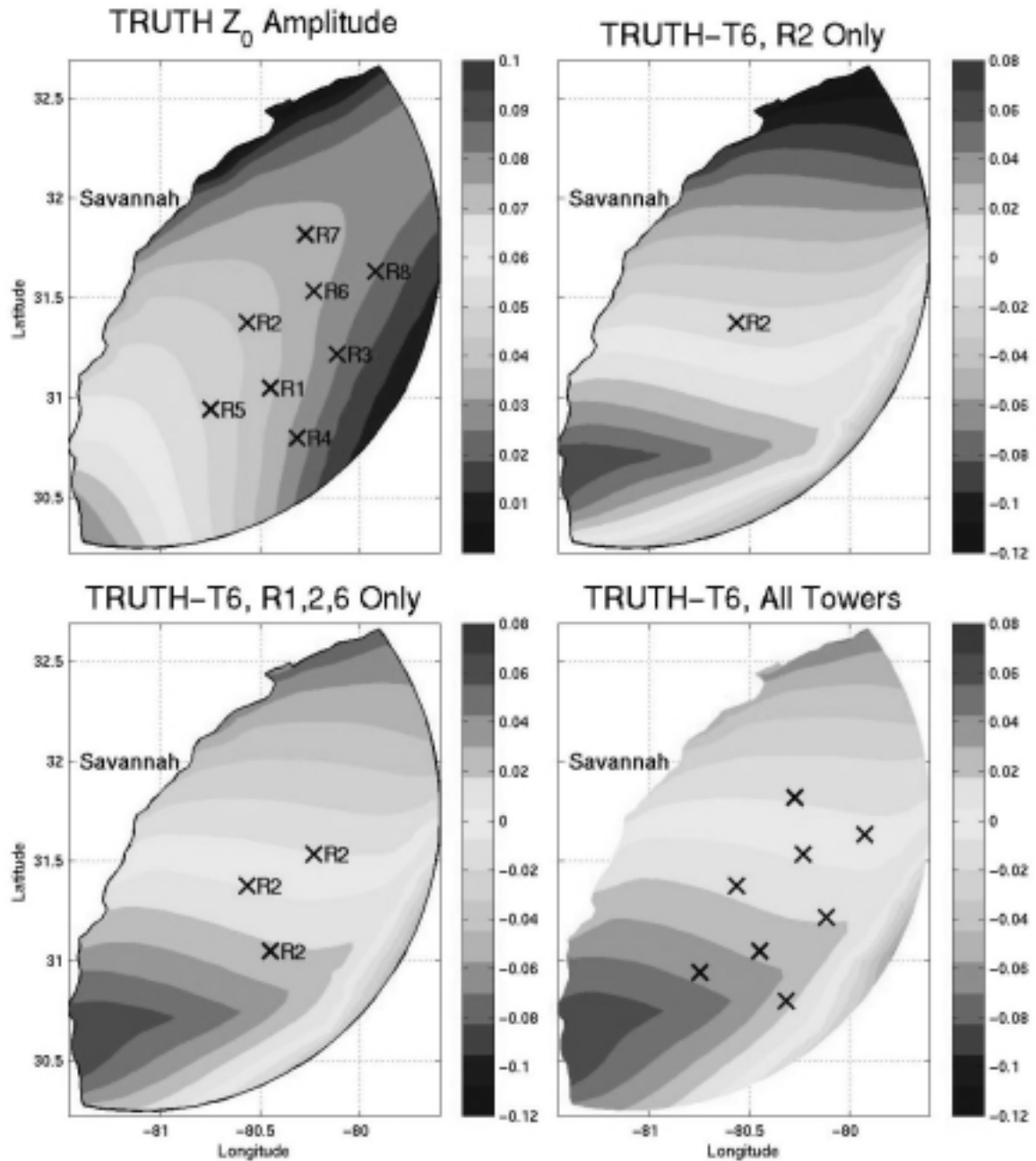


Figure 21. Steady (zero-frequency) sea surface elevation. True solution, top left (a); true minus solution computed with one tower, top right (b); true minus solution computed with three towers, bottom left (c); and true minus solution computed with eight towers, bottom right (d). Note that the scale of the true solution is different from the difference between true and computed.

Atmospheric Deposition

During the initial phase of the SABSOON project, simple funnel atmospheric deposition collectors have been maintained on the SkIO campus and on the R2 and R3 offshore towers. These collectors consist of simple plastic funnels connected to storage bottles. The storage bottles are blackened to minimize potential photochemical oxidation and transformation of the different nitrogen species. To reduce microbial activity, 5 ml of 12 N HCl is added to each bottle prior to deployment.

To date, continuous collections of 890, 779, and 614 days have been made at the SkIO, R2 and R3 locations, respectively. Individual collection periods averaged roughly 30 days, although actual collection periods ranged from 119 to 21 days depending on the availability of the helicopters. To examine potential biases that may be due to the large radar truss on the towers, two collectors were maintained on opposite sides of the towers (Designated as locations A and B).

Measured deposition rates at each location display considerable variability. At SkIO, individual values range from 100 to 1898 $\mu\text{mol N m}^{-2} \text{d}^{-1}$ with an average daily rate of 710 $\mu\text{mol m}^{-2} \text{d}^{-1}$. At tower R2, values ranged from 64 to 1531 $\mu\text{mol m}^{-2} \text{d}^{-1}$ with an average of 727 and 706 at the A and B locations, respectively. At tower R3, values ranged from 149 to 1417 $\mu\text{mol m}^{-2} \text{d}^{-1}$ with an average of 797 and 750 $\mu\text{mol m}^{-2} \text{d}^{-1}$ at the A and B locations, respectively. Thus, while there is extensive variability within individual measurements, the mean values for all sampling locations are quite consistent, ranging from 706 (R2B) to 797 (R3A).

Most of the variability is attributed to the episodic nature of rain events in the SAB region that are presumed to account for most of the flux. Despite collecting samples over extended time periods (30 days) which would integrate over many of the individual rain events, significant variability remains. Examination of correlations with wind direction is just beginning. Another possible source of variability would be episodic contaminant by bird droppings in our collection funnels. We have assessed this possibility by determining the phosphorus content of the samples. Because guano is enriched in phosphorus, elevated phosphorus concentrations are a sensitive indicator of possible contamination. Phosphorus concentrations were generally low, nominally less than 2-3 μM . Thus, we conclude that the elevated N concentrations are not caused by contamination by birds. In rough terms, the observed level of atmospheric nutrient input is 10 times the riverine input and a tenth of the input associated with Gulf Stream intrusions. It appears that atmospheric deposition is an important nutrient source for the mid-shelf region.

Distribution of Real-time Observations

The observations are currently distributed in two ways. The SABSOON website (<http://www.skio.peachnet.edu/projects/sabsoon.html>) includes a section devoted to tabular and graphical presentation of the last months observations from all the data streams (except for the video camera imagery). The observations on the website are updated hourly. This simple presentation of the observations is an invaluable tool for monitoring episodic events on the shelf and for identifying any problems with the various sensors. Improvements to the website

occur regularly, in response to the deployment of new instrumentation, and as methods for streamlining processing and presentation of the observations are discovered.

Observations are also reported to the National Weather Service (NWS). The towers have been designated as part of the Coastal Marine Automated Network (CMAN) program. Each hour observations of interest are properly formatted and transmitted to the NWS in Houston, Texas (the regional office for the southeast). From there the Jacksonville Florida NWS office passes the observations through the World Meteorological Organizations Telecommunications gateway, making the observations available worldwide. The observations fill a critical gap in the national observational network along the southeastern seaboard (Dr. P. Welsh, NWS Jacksonville, pers. Comm.).

References

- Atkinson, L. P., T. N. Lee, J. O. Blanton and W. S. Chandler, 1983. Climatology of the southeastern United States continental shelf waters, *J. Geophys. Res.-Oceans* **88**: 4705-4718.
- Blanton, J. O., 1981. Ocean currents along a nearshore frontal zone of the continental shelf of the southeastern United States, *J. Phys. Oceanogr.* **11**: 1627-1637.
- Blanton, J.O., L.-Y. Oey, J. Amft and T.N. Lee, 1989. Advection of momentum and buoyancy in a coastal frontal zone. *J. Phys. Oceanogr.* **19**: 98-115.
- Blanton, J. O., 1996. Reinforcement of gravitational circulation by wind, in *Buoyancy effects on coastal and estuarine dynamics*, Coastal and estuarine studies Vol. 53, Amer. Geophys. Union, 47-58.
- Chen, C., L.Y. Zheng and J.O. Blanton, 1999. Physical processes controlling the formation, evolution, and perturbation of the low-salinity front in the inner shelf off the southeastern United States: A modeling study. *J. Geophys. Res.-Oceans* **104**: 1259-1288.
- Cooper, C. K., G. Z. Forristall, R. C. Hamilton and C. C. Ebbesmeyer, 1993. Utilization of Offshore Oil Platforms for Meteorological and Oceanographic Measurements, *Marine Tech. Soc. Jour.*, **27**: 10-23.
- Hosom, D. S., R. A. Weller, R. E. Payne and K. E. Prada, 1995. The IMET (Improved Meteorology) Ship and Buoy Systems, *Jour. Atmos. Oceanic Tech.*, **12**: 527-540.
- Jahnke, R.J, J.R. Nelson, R.L. Marinelli and J.E. Eckman, 2000. Benthic flux of biogenic elements on the Southeastern U.S. continental shelf: Influence of pore water advective transport and benthic microalgae. *Cont. Shelf Res.* **20**: 109-127.
- Lee, T. N., V. Kourafalou, J. D. Wang, W. J. Ho., J. O. Blanton, L. P. Atkinson and L. J. Pietrafesa, 1985. Shelf circulation from Cape Canaveral to Cape Fear during winter, *in* *Oceanography of the southeastern U. S. continental shelf*, L. Atkinson, D. Menzel and K. Bush, eds, Amer. Geophys. Union, 63-76.
- Moran, M.A. and R.G. Zepp, 1997. Role of photoreactions in the formation of biologically labile compounds from dissolved organic matter. *Limnol. Oceanogr.* **42**: 1307-1316.
- Nelson, J.R. and S. Guarda, 1995. Particulate and dissolved spectral absorption on the continental shelf of the southeastern United States. *J. Geophys. Res.* **100**: 8715-8732.
- Nelson, J.R., J.E. Eckman, C.Y. Robertson, R.L. Marinelli and R.A. Jahnke, 1999. Benthic microalgal biomass and irradiance at the sea floor on the continental shelf of the South Atlantic Bight: Spatial and temporal variability and storm effects. *Cont. Shelf Res.* **19**: 477-505.
- Pietrafesa, L. J., J. O. Blanton, J. D. Wang, V. Kourafalou, T. N. Lee and K. A. Bush, 1985. The tidal regime in the South Atlantic Bight, *in* *Oceanography of the southeastern U. S. continental shelf*, L. Atkinson, D. Menzel and K. Bush, eds, Amer. Geophys. Union, 63-76.
- Pond, S. and G. L. Pickard, 1983. *Introductory dynamical oceanography*, Pergamon Press, Elmsford, New York, 329 pp.
- Seim, H.E., 2000. Implementation of the South Atlantic Bight Synoptic Offshore Observational Network. *Oceanography* **13**(2): 18-23.

Weber, A. H. and J. O. Blanton, 1980. Monthly mean wind fields for the South Atlantic Bight. *Jour. Phys. Oceanogr.*, **10**: 1256-1263.

Weller, R. A. and S. P. Anderson, 1996. Surface Meteorology and Air-Sea Fluxes in the western equatorial pacific warm pool during the TOGA coupled ocean-atmosphere response experiment, *Jour. Climate*, **9**: 1959-1990.